ADVANCED FUNCTIONAL MATERIALS
www.afm-journal.de

Multifunctional Mesoporous Silica Nanoparticles for Cancer-Targeted and Controlled Drug Delivery

*Quan Zhang, Fang Liu, Kim Truc Nguyen, Xing Ma, Xiaojun Wang, Bengang Xing, and Yanli Zhao**

Multifunctional mesoporous silica nanoparticles are developed in order to deliver anticancer drugs to specific cancer cells in a targeted and controlled manner. The nanoparticle surface is functionalized with amino-β-cyclodextrin rings bridged by cleavable disulfide bonds, blocking drugs inside the mesopores of the nanoparticles. Poly(ethylene glycol) polymers, functionalized with an adamantane unit at one end and a folate unit at the other end, are immobilized onto the nanoparticle surface through strong β-cyclodextrin/adamantane complexation. The non-cytotoxic nanoparticles containing the folate targeting units are efficiently trapped by folate-receptor-rich HeLa cancer cells through receptor-mediated endocytosis, while folate-receptor-poor human embryonic kidney 293 normal cells show much lower endocytosis towards nanoparticles under the same conditions. The nanoparticles endocytosed by the cancer cells can release loaded doxorubicin into the cells triggered by acidic endosomal pH. After the nanoparticles escape from the endosome and enter into the cytoplasm of cancer cells, the high concentration of glutathione in the cytoplasm can lead to the removal of the β-cyclodextrin capping rings by cleaving the pre-installed disulfide bonds, further promoting the release of doxorubicin from the drug carriers. The high drug-delivery efficacy of the multifunctional nanoparticles is attributed to the co-operative effects of folate-mediated targeting and stimuli-triggered drug release. The present delivery system capable of delivering drugs in a targeted and controlled manner provides a novel platform for the next generation of therapeutics.

1. Introduction

A major challenge to a successful cancer chemotherapy is how to achieve specific drug accumulation at tumor sites.[1] Conventional chemotherapeutic agents are distributed non-specifically in the body where they affect both cancerous and normal cells, thereby limiting the dose achievement within tumors and also resulting in systemic toxicity and undesired side effects.[2] In order to improve the chemotherapy, tremendous research efforts have been devoted to the development of tumor-targeted nanocarriers for the controlled delivery of anticancer drugs such as doxorubicin (Dox).[3–7] Various nanocarrier platforms, including liposomes, polymeric nanoparticles, nanomicelles, and dendrimers, have been developed in order to deliver anticancer drugs to tumor tissues by taking advantage of the enhanced permeation and retention (EPR) effect.[8–12] The surfaces of these nanocarriers are often functionalized with poly(ethylene glycol) (PEG) polymers. Surface modifications with PEG offer several unique features, including the enhancement of the nanocarrier dispersion in physiological conditions, the prolongation of the nanocarrier circulation time in blood, and the facilitation of preferential accumulation at the tumor sites by the EPR effect.[13,14]

The EPR effect is often not efficient enough to eradicate the side effects of cytotoxic drugs and to exert the anticancer therapy selectively in cancer cells.[1] In order to further enhance the targeting ability of nanocarriers to cancer cells, a promising strategy is to functionalize the surface of nanocarriers using the targeting agents that can selectively bind to over-expressed antigens or receptors on the surface of cancer cells.[1,15] The targeting agents normally include antibodies (*e.g.*, monoclonal antibody),[16] peptides (*e.g.*, Arg-Gly-Asp (RGD)),[17] and small molecules (*e.g.*, folate).[18]

An ideal drug delivery system should be stable under a long circulation period, and can keep loaded drugs unreleased during the circulation in the bloodstream or in normal tissues. Upon reaching and accumulating in tumor tissues by passive and active targeting, and after being taken up by cancer cells, the system should release the drugs rapidly in response to the local environment. Mesoporous silica nanoparticles (MSNPs) have attracted much attention since they can serve as novel nanocarriers for on demand drug delivery.[19–23] Major research on MSNPs has thus far focused on the development of controlled cargo release in response to external stimuli such as redox,[24–26]

Dr. Q. Zhang, F. Liu, K. T. Nguyen, Dr. X. Wang, Prof. B. Xing, Prof. Y. L. Zhao
Division of Chemistry and Biological Chemistry
School of Physical and Mathematical Sciences
Nanyang Technological University
21 Nanyang Link, Singapore 637371
E-mail: zhaoyanli@ntu.edu.sg
X. Ma, Prof. Y. L. Zhao
School of Materials Science and Engineering
Nanyang Technological University
50 Nanyang Avenue, Singapore 639798

DOI: 10.1002/adfm.201201316

pH changes,[27–29] enzyme actions,[30–32] and photoirradiation.[33] pH-Responsive drug delivery strategy is frequently used, as pH values in different tissues and cellular compartments vary tremendously. For example, the extracellular environment in tumor tissues is more acidic (pH 6.5) than that in blood and normal tissues (pH 7.4), and the pH values of endosome and lysosome in cancer cells are even lower at 5.0–5.5.[34,35] Various pH-responsive delivery systems have been developed in order to accomplish pH-triggered drug release in tumor tissues.[28,29,36] However, the drug release triggered only by pH changes is often insufficient to maximize the drug delivery efficacy and to minimize the side effects of anticancer drugs.

Herein, we report the development of novel multifunctional MSNPs for cancer-targeted and controlled drug delivery. The multifunctional MSNPs can be efficiently trapped by cancer cells through receptor-mediated endocytosis, and release loaded anticancer drugs rapidly triggered by acidic endosomal pH and intracellular glutathione. Several functions were built into the multifunctional MSNPs in order to deliver drugs in an optimal fashion. These functions include (i) PEGylated coating on the nanoparticle surface to enhance long-term stability of the nanoparticles under physiological conditions, (ii) active cancer targeting by the folate ligands attached on the nanoparticle surface, (iii) pH-triggered drug release to allow drugs released within acidic intracellular compartments such as endosome and lysosome (pH 5.0–5.5), (iv) positively charged nanoparticle surface under acidic condition to facilitate the transfer of the nanoparticles from endosome to cytoplasm, and (v) glutathione-induced cleavage of the disulfide bonds to further enhance the drug release in the cytoplasm of cancer cells. The engineering of multifunctional MSNPs with these functionalities in single nanoparticle entities can significantly enhance the efficacy of anticancer drug delivery, and reduce the cytotoxicity to healthy cells. We also demonstrated that the high drug delivery efficacy of multifunctional nanoparticles is attributed to the cooperative effects of folate-mediated targeting and stimuli-triggered drug release.

The structure and delivery strategy of multifunctional MSNPs are illustrated in **Figure 1**. MSNPs were initially prepared by following a base-catalyzed sol-gel procedure.[37] The surface of MSNPs was then functionalized with mercaptopropyl groups by refluxing MSNPs with 3-mercaptopropyltrimethoxysilane (MPTMS) in order to afford sulphydryl-functionalized MSNPs (MSNPs-SH-0), which were further reacted with 2-carboxyethyl-2-pyridyl disulfide to yield the carboxylic acid-functionalized nanoparticles. After the removal of the surfactant (cetyltrimethylammonium bromide, CTAB), cargo molecules (*e.g.* doxorubicin) were loaded into the mesopores followed by the functionalization of per-diamino-β-cyclodextrin (β-CD$(NH_2)_7$) on the nanoparticle surface via the amidation, leading to β-CD$(NH_2)_7$ modified MSNPs (MSNPs-S-S-CD, Figure 1a). The β-CD ring serving as a gate can physically block the mesopore orifice,[27] keeping the cargo molecules inside the mesopores. Two types of poly(ethylene glycol) (PEG) derivatives were synthesized, namely, methoxyl PEG polymer functionalized with the adamantane (Ad) unit (mPEG-Ad), and PEG polymer functionalized with Ad unit at one end and folate unit at the other end (FA-PEG-Ad). A mixture of mPEG-Ad and FA-PEG-Ad was immobilized (Figure 1b) onto the surface of MSNPs-S-S-CD through strong Ad/β-CD complexation in aqueous solution,[38,39] offering the FA targeting unit on the surface of the nanoparticles. Since the folate receptor (FR) has been found to be over-expressed on the surfaces of brain, kidney, lung, and breast cancer cells,[40,41] the multifunctional MSNPs containing the FA targeting units can be selectively trapped by the FR-rich cancer cells through receptor-mediated endocytosis, making the controlled intracellular drug delivery applicable.

2. Results and Discussion

2.1. Preparation and Characterization of Multifunctional MSNPs

Transmission electron microscopy (TEM) images provide direct evidence for the formation of multifunctional MSNPs. As shown in **Figure 2**a, the diameter of the as-synthesized MSNPs is around 100 nm with 2–3 nm of the mesopore size. When the nanoparticles were incorporated with the β-CD rings and mPEG-Ad/FA-PEG-Ad polymers, the nanoparticle shape (Figure 2b,c) did not change significantly, indicating that the nanoparticles can still keep their morphology after the functionalization. In addition, the mesopore arrays on the nanoparticles cannot be clearly observed after the introduction of the PEG polymers in aqueous solution, because of the masking of the polymers (Figure 2d).

A specific surface area of 967 $m^2\ g^{-1}$ and an average mesopore diameter of 2.8 nm for the as-synthesized MSNPs were observed by Brunauer-Emmett-Teller (BET) analysis and Barret-Joyner-Halenda (BJH) analysis, respectively (Figure S1 in the Supporting Information (SI)). Powder X-ray diffraction (XRD) analysis shows that the as-synthesized MSNPs possess well-ordered porous structures with typical MCM-41-type hexagonal arrangements (Figure S2 in the SI). A series of surface functionalizations on MSNPs were confirmed by ^{13}C and ^{29}Si cross-polarization magic-angle-spinning (CP-MAS) solid-state NMR spectroscopy. Examination on the ^{13}C CP-MAS solid-state NMR spectrum of MSNPs-S-S-CD (**Figure 3**) indicates that (i) the signals resonating between 12 and 50 ppm are attributed to characteristic peaks of aliphatic carbons on the linker between the β-CD ring and the nanoparticle, (ii) the signals resonating between 50 and 105 ppm are assigned to characteristic carbon peaks on the β-CD skeleton, and (iii) the signal resonating around 170 ppm is attributed to characteristic peak of the amide carbonyl carbon. The ^{29}Si CP-MAS solid-state NMR spectrum of MSNPs-S-S-CD presents two silicon peaks around −60 and −105 ppm, corresponding to the functionalized silica (T region) and bulk silica (Q region), respectively.[42]

In order to confirm that the Ad-conjugated PEG polymers can be immobilized onto MSNPs-S-S-CD via the Ad/β-CD complexation, MSNPs-S-S-CD was stirred with mPEG-Ad in aqueous solution for 12 h. The PEG-coated nanoparticles were obtained by centrifugation and washed with H_2O in order to remove the excess polymers. The weight percentages of the β-CD$(NH_2)_7$ and mPEG-Ad units on the nanoparticles measured by thermogravimetric analysis are 3.0% and 5.7%, respectively (Figure S3 in the SI).

Dynamic light scattering (DLS) and zeta potential experiments further confirm the successful surface functionalization

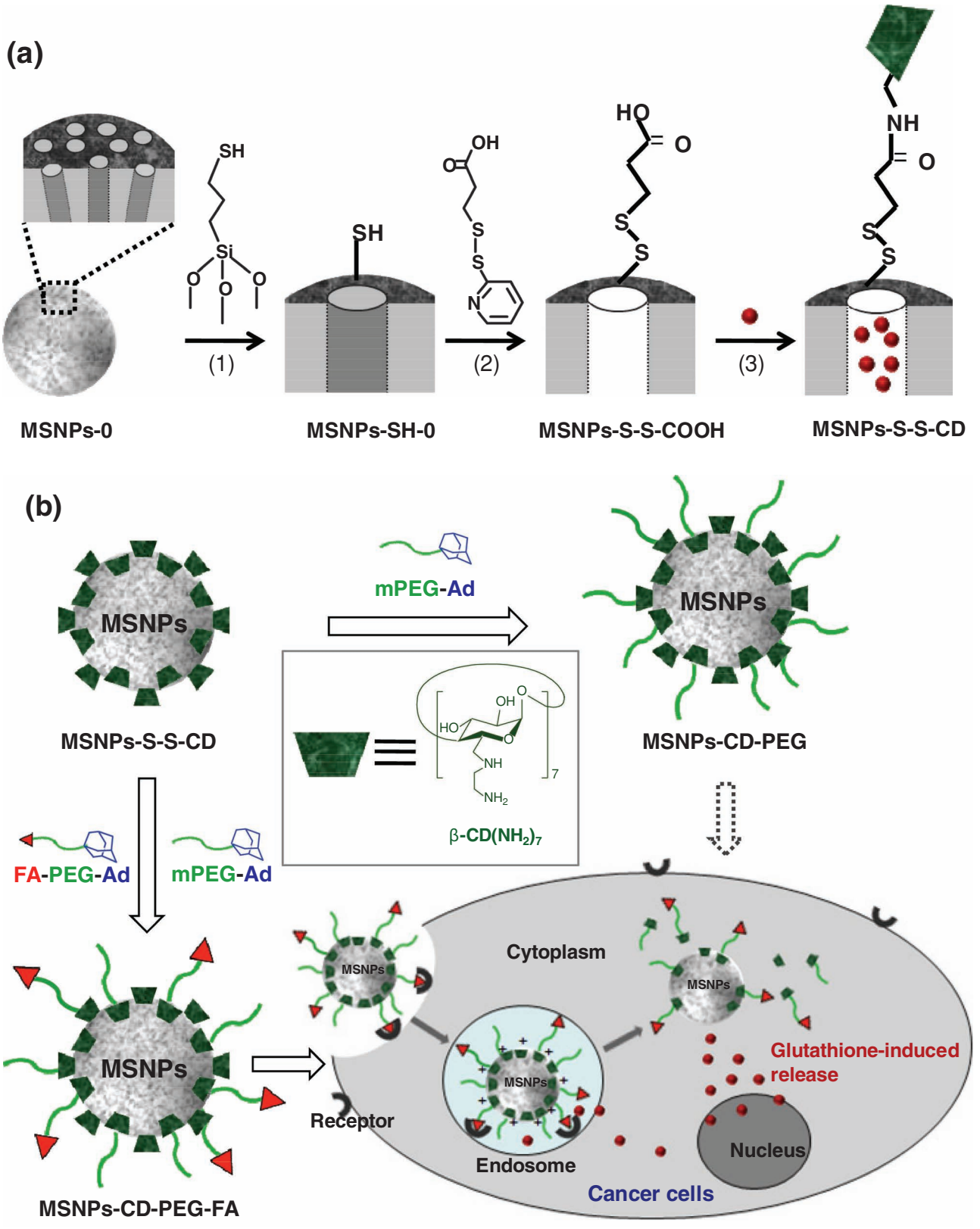

Figure 1. a) Synthetic representation of the cargo-loaded MSNPs-S-S-CD. Reaction conditions: (1) MPTMS in toluene; (2) 2-carboxyethyl-2-pyridyl disulfide in ethanol, followed by the removal of the surfactant CTAB; (3) loading of cargo molecules, followed by additions of β-CD$(NH_2)_7$ and 1-(3-(dimethylamino)propyl)-3-ethylcarbodiimide hydrochloride (EDC·HCl). MSNPs-0 and MSNPs-SH-0 mean that the mesopores are occupied with the CTAB template. b) Schematic illustration of multifunctional MSNPs-CD-PEG-FA for targeted and controlled drug delivery.

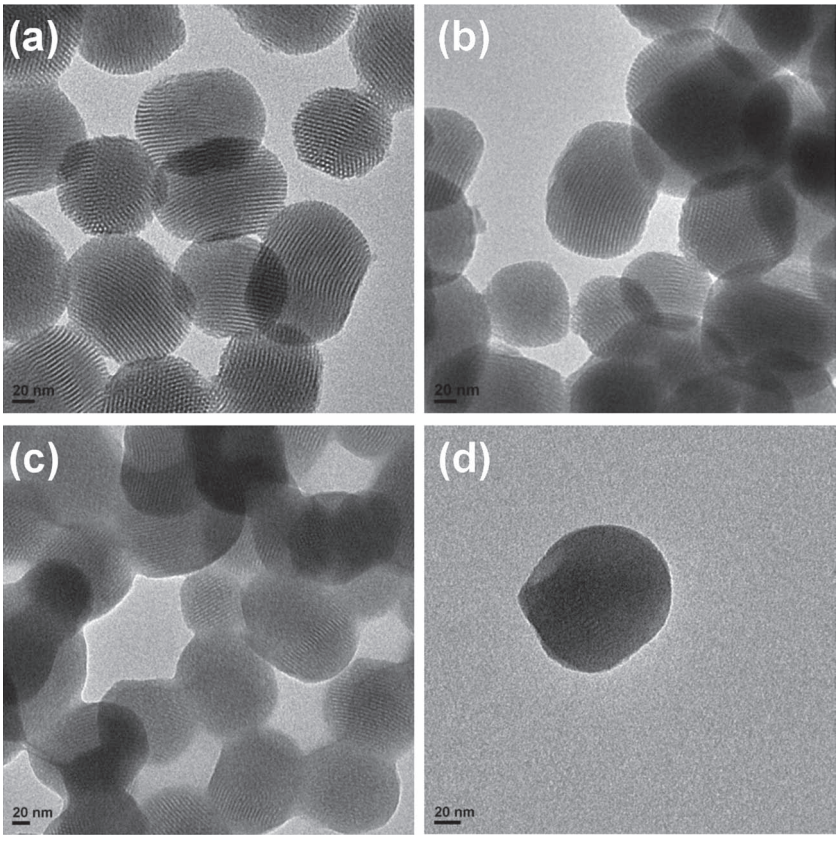

Figure 2. TEM images of: a) MSNPs, b) MSNPs-S-S-CD, and c,d) MSNPs-CD-PEG-FA prepared in aqueous solution.

of MSNPs (Table S1 in the SI). The aqueous dispersion of as-synthesized MSNPs showed a low stability after the samples were kept at room temperature for 30 min. The DLS data show that MSNPs exhibit a hydrodynamic diameter of 1145 nm (PDI 0.805) as a result of the nanoparticle aggregation in H_2O. The introduction of the PEG polymers can improve the colloidal stability of MSNPs in H_2O or phosphate buffered saline (PBS) solution. MSNPs-CD-PEG presents a narrow size distribution with an overall hydrodynamic diameter of 203.3 nm (PDI 0.229) in H_2O (**Figure 4**a). MSNPs-CD-PEG can retain its narrow size distribution even in culture media containing 10% fetal bovine serum (FBS). The long-term stability of MSNPs-CD-PEG was evaluated by suspending the nanoparticles in PBS solution (pH 7.4) and culture media containing 10% FBS, respectively. No significant size change was observed after incubation of MSNPs-CD-PEG in these media for at least 6 days (Figure 4b,c), demonstrating an excellent colloidal stability of MSNPs-CD-PEG under physiological conditions. In the zeta potential measurements, MSNPs-S-S-COOH in H_2O offers a negative zeta potential (–40.9 ± 0.8 mV) attributed from the carboxyl groups on the nanoparticle surface. The surface charge was reversed to a positive value (+19.8 ± 0.2 mV) in H_2O after the β-CD$(NH_2)_7$ ring was covalently linked onto the nanoparticles (MSNPs-S-S-CD). Since excess β-CD$(NH_2)_7$ molecules were used to react with MSNPs-S-S-COOH in order to maximize the amount of β-CD$(NH_2)_7$ capped on the nanoparticles, the unreacted amino groups of β-CD$(NH_2)_7$ on MSNPs-S-S-CD afford a positive zeta potential in H_2O. The introduction of the PEG polymers onto the nanoparticle system

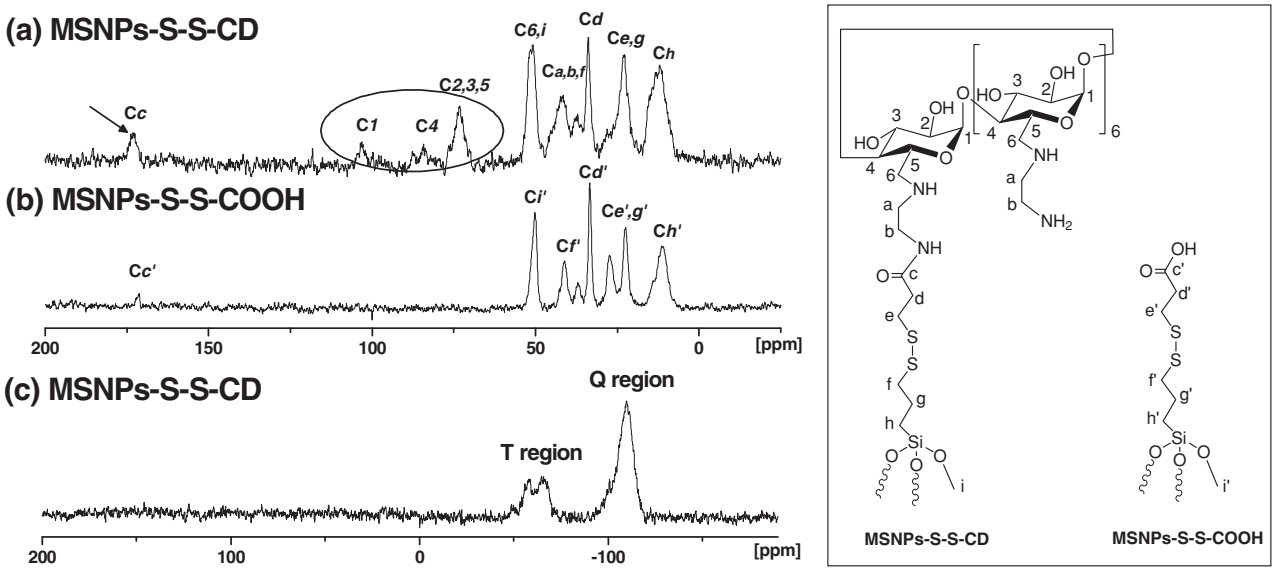

Figure 3. a) ^{13}C CP-MAS solid-state NMR spectrum of MSNPs-S-S-CD. b) ^{13}C CP-MAS solid-state NMR spectrum of MSNPs-S-S-COOH. c) ^{29}Si CP-MAS solid-state NMR spectrum of MSNPs-S-S-CD.

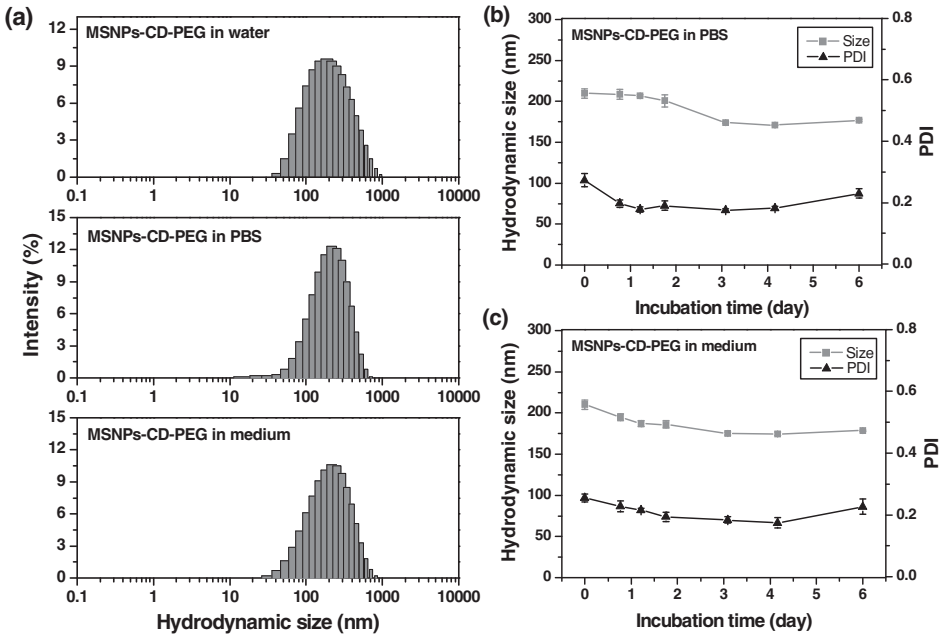

Figure 4. a) Hydrodynamic size distribution of MSNPs-CD-PEG in water, PBS (pH 7.4), and culture medium with 10% serum. b,c) Long-term colloidal stability of MSNPs-CD-PEG in the presence of PBS buffer solution (pH 7.4) (b) or culture medium containing 10% FBS (c). The error bars were obtained from three independent measurements.

does not significantly affect the zeta potential in H_2O as compared with that of MSNPs-S-S-CD.

2.2. Drug Loading and Release Studies

To investigate the stimuli-triggered drug release of the MSNPs-S-S-CD system, Dox was first loaded into MSNPs-S-S-COOH (4 mg mL^{-1}) in solution. β-CD$(NH_2)_7$ (30 mg, 0.021 mmol) was then added to the Dox-loaded MSNPs-S-S-COOH nanoparticles (20 mg) in the presence of 1-(3-(dimethylamino) propyl)-3-ethylcarbodiimide hydrochloride (EDC·HCl, 15 mg, 0.078 mmol) in H_2O (10 mL). After the reaction mixture was stirred for 48 h, the resulting nanoparticles were collected by centrifugation, washed extensively with PBS (pH 7.4), and finally dried under vacuum. The procedure ensures that there are no potential complexation between Dox and β-CD$(NH_2)_7$ and no reaction between the carboxylic acid unit of MSNPs-S-S-COOH and amino group of Dox during the preparation process. The loading percentage of Dox in MSNPs-S-S-CD determined by UV-Vis absorption measurement is 4.8%.

As the β-CD rings were attached onto the nanoparticle surface via disulfide bonds, the capping rings can be removed by the cleavage of the disulfide bonds in the presence of reduction agents, thus leading to the controlled release of Dox from the mesopores. Dithiothreitol (DTT) and glutathione (GSH) were employed as reduction agents to trigger the redox-responsive release of Dox. Dox-loaded MSNPs-S-S-CD (3 mg) was placed in a cuvette, which was then carefully filled with PBS buffer (3 mL, pH 7.4). The concentration of released Dox was calculated by the measurement of fluorescence intensity at 593 nm (λ_{ex} = 480 nm) with reference to the standard curve. As shown in **Figure 5**a, very weak fluorescence intensity was observed in solution in the absence of DTT or GSH, indicating that the β-CD rings on the nanoparticle surface can effectively block Dox within the mesopores. Upon the addition of reduction agent DTT or GSH, the rapid release of Dox from the nanoparticles was observed, since the disulfide bonds between the β-CD rings and MSNPs were broken and the β-CD rings were removed from the surface.

Interestingly, the Dox release rate induced by DTT is slower as compared with that by GSH. Since GSH has a lower p*K*a (3.59) than that of DTT (p*K*a 9.2), the observation suggests that Dox-loaded MSNPs-S-S-CD is sensitive to acidic environment. Indeed, when the solution pH was adjusted to acidic conditions, significant release of Dox was observed (Figure 5b). As the unreacted amino groups of β-CD$(NH_2)_7$ on the nanoparticles are protonated to ammoniums under acidic conditions, the Coulombic repulsion between the positively charged β-CD rings around the nanoparticle orifices leads to the opening of the mesopores, facilitating the release of positively charged Dox. In order to prove the hypothesis, negatively charged calcein was loaded into MSNPs-S-S-CD instead of positively charged Dox. A quick calcein release from the nanoparticles was observed at pH 7.4 as compared with those under acidic conditions (Figure S4 in the SI), the observation which is opposite to the release of positively charged Dox. The reason is that the electrostatic attraction between the positively charged β-CD rings and negatively charged calcein under acidic conditions will result in the slow cargo release.[43] In another control experiment, when MSNPs-S-S-COOH was employed to load Dox under the same conditions, Dox-loaded MSNPs-S-S-COOH showed a fast Dox release rate at 37 °C independent of the pH values or the GSH addition (Figure 5d), further supporting the conclusion that the β-CD$(NH_2)_7$ rings on MSNPs-S-S-CD can control the loading and release of the drug molecules in the mesopores upon the

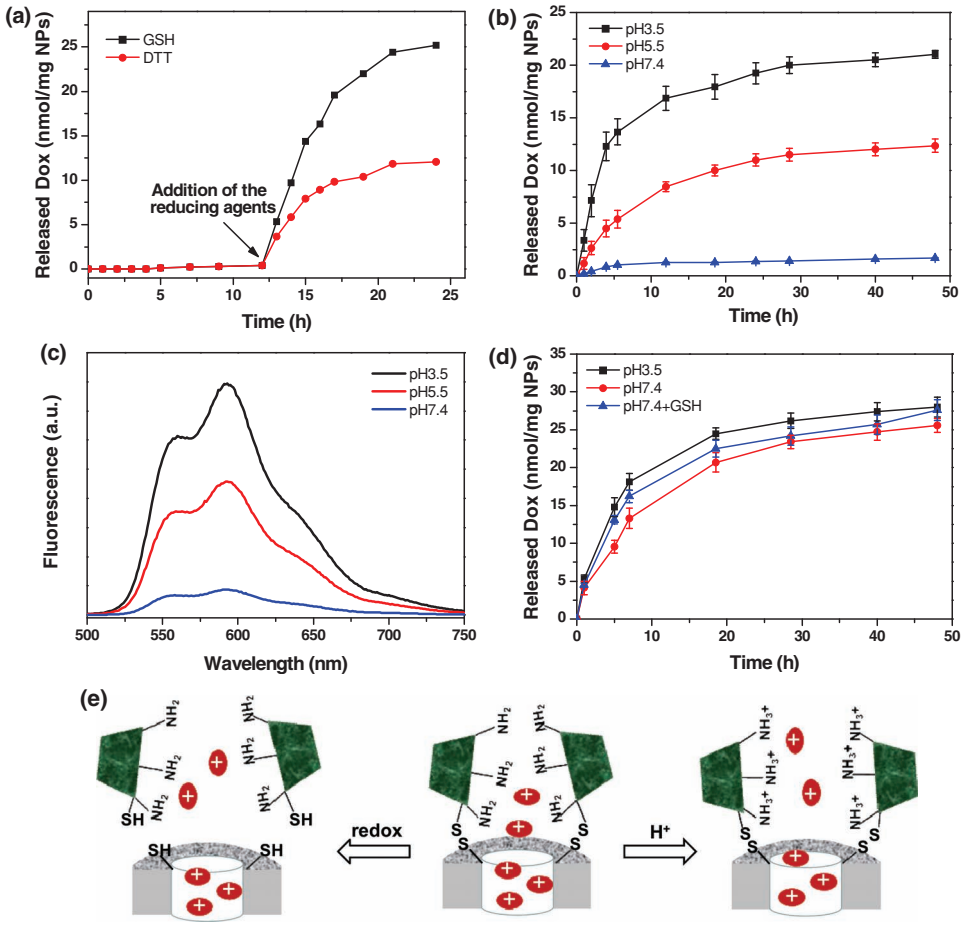

Figure 5. a) Release profiles of Dox-loaded MSNPs-S-S-CD in PBS (pH 7.4) triggered by the addition of DTT (10 mM) or GSH (10 mM). b) Release profiles of Dox-loaded MSNPs-S-S-CD at 37 °C under different pH conditions. c) Fluorescence spectra of Dox (λ_{ex} = 480 nm) after 40 h incubation of Dox-loaded MSNPs-S-S-CD at different pH values. d) Release profiles of Dox-loaded MSNPs-S-S-COOH at 37 °C under different pH conditions. The Dox release was not affected by the addition of GSH (10 mM). e) Dual release mechanism of Dox-loaded MSNPs-S-S-CD. Drug release of Dox-loaded MSNPs-S-S-CD can be triggered by acidic pH or the addition of a reduction agent such as DTT or GSH.

pH changes. Thus, Dox can be released either by the introduction of reduction agents (i.e., intracellular GSH) to cleave the disulfide bonds, or by the electrostatic repulsion triggered by acidic pH (Figure 5e).

2.3. Folate-Mediated Endocytosis

In order to verify the feasibility of MSNPs-S-S-CD as targeted drug delivery carriers in biological systems, green emitting fluorescein labeled MSNPs-S-S-CD (FMSNPs-S-S-CD) was synthesized to provide a means for fluorescent tracing.[44] As a mixture of mPEG-Ad and FA-PEG-Ad can be immobilized on FMSNPs-S-S-CD through strong Ad/β-CD complexation, the surface coverage of FA on the nanoparticles can be mediated by varying the molar ratio between FA-PEG-Ad and mPEG-Ad. Flow cytometry experiment was carried out to evaluate the cell uptake of FMSNPs-S-S-CD by FR-positive HeLa cells under different surface coverages of the FA ligands (Figure S5 in the SI). The obtained data demonstrated an increase in the cell uptake of FMSNPs-S-S-CD upon an increase in the molar ratio of FA-PEG-Ad to mPEG-Ad. The maximum nanoparticle uptake was observed when the molar ratio of FA-PEG-Ad to mPEG-Ad reaches 1:1 (i.e., FA-PEG-Ad added about 50 mol% of the total polymer content), indicating a saturation binding of the nanoparticles to cells under this FA surface coverage.

In order to confirm the folate-mediated endocytosis of multifunctional nanoparticles, a mixture of mPEG-Ad and FA-PEG-Ad (1:1 mol ratio) was immobilized onto FMSNPs-S-S-CD through the Ad/β-CD complexation, leading to the nanoparticles FMSNPs-CD-PEG-FA. FMSNPs-S-S-CD coated only with mPEG-Ad was also prepared as a control sample (FMSNPs-CD-PEG). FR-positive human cervical carcinoma HeLa cells cultured in an FA-free medium and FR-negative human embryonic kidney (HEK) 293 cells cultured in a normal medium were incubated with either FMSNPs-CD-PEG or FMSNPs-CD-PEG-FA (20 μg mL^{-1}) for fluorescence imaging investigations (**Figure 6**a). The indirect immunostaining methods were used to confirm the over-expression of α-folate receptor on HeLa cells, but not on 293 cells (Figure 6c). To ensure the green

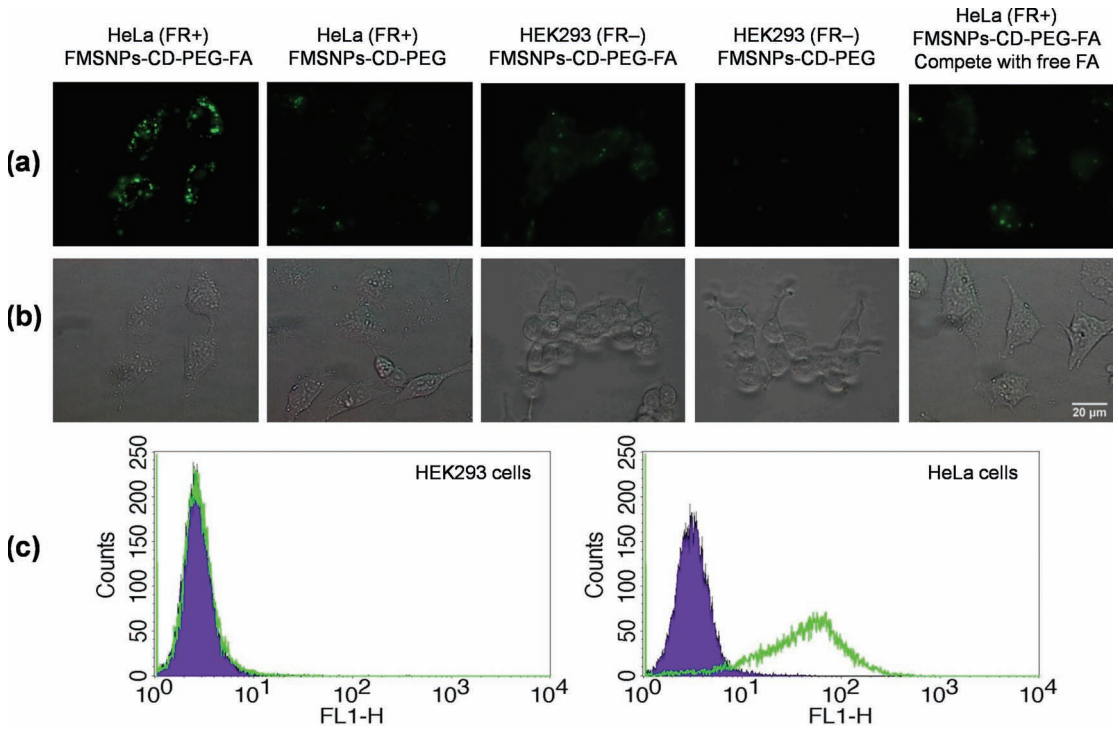

Figure 6. a) Fluorescence images and b) bright-field images of HeLa cells and 293 cells after 3 h incubation with either FMSNPs-CD-PEG-FA or FMSNPs-CD-PEG as indicated. After Trypan blue was used to quench the extracellular fluorescence, the cells were monitored live by fluorescence microscopy. c) Flow cytometry analyses show that the α-folate receptor was over-expressed on HeLa cells, but not on 293 cells. Surface expression of the folate receptor was evaluated by indirect immunostaining using the anti-folate receptor primary antibody (Mov18, 2 μg mL^{-1}) followed by using ATTO488 conjugated anti-mouse secondary antibody (green line). Non-specific fluorescence was assessed using the secondary antibody only (purple area). The results are representative of two independent experiments.

fluorescence observed was indeed from FMSNPs-S-S-CD that was endocytosed, the extracellular fluorescence was quenched with trypan blue.[45] A strong green fluorescence was observed from HeLa cells incubated with FMSNPs-CD-PEG-FA, while HeLa cells incubated with FMSNPs-CD-PEG showed negligible nonspecific binding. No obvious fluorescence was observed from 293 cells after the incubation with either FMSNPs-CD-PEG-FA or FMSNPs-CD-PEG. When HeLa cells incubated with both FMSNPs-CD-PEG-FA and free FA under the same conditions, a very weak fluorescence was observed on account of the FR competition. To quantitatively measure the FMSNPs-CD-PEG-FA uptake by HeLa cells in the presence and absence of the competition of free FA, flow cytometry experiment was carried out to quantify the mean fluorescence intensity (MFI) from HeLa cells (Figure S6 in the SI). When adding 1 mM of free FA, the MFI value decreased to half of the value measured in the absence of free FA, demonstrating (i) a statistically significant inhibition of the nanoparticle uptake by free FA and (ii) the specific FR-mediated targeting of FMSNPs-CD-PEG-FA for cancer cells.

2.4. Endosomal Escape

The intracellular distribution of FMSNPs-CD-PEG-FA was further evaluated by confocal laser scanning microscopy (CLSM). A red Lysotracker probe was used to stain the acidic organelles in HeLa cells. We found that FMSNPs-CD-PEG-FA was dominantly localized in Lysotracker-labeled acidic organelles after 3 h of incubation (**Figure 7**a). Those nanoparticles that were trapped inside endosome/lysosome are yellow in color, which is the result of the overlap between red (Lysotracker) and green (FMSNPs) spots. Nevertheless, some of the FMSNPs-CD-PEG-FA nanoparticles appeared to be able to escape from the endosome after 24 h, and were distributed in the cytoplasm (Figure 7b). The amino groups of β-CD$(NH_2)_7$ on the nanoparticles were protonated at acidic endosomal pH, which disrupt the endosome and promote the escape of the nanoparticles from the endosome into the cytoplasm. The behavior can be attributed to the "proton-sponge" or "endosome buffering" effect.[46,47]

2.5. Intracellular Drug Release

Following cellular internalization, another key issue is whether Dox can be efficiently released from Dox-loaded FMSNPs-CD-PEG-FA. To visualize intracellular Dox release, the cellular uptake of Dox-loaded FMSNPs-CD-PEG-FA was further investigated by confocal laser scanning microscopy (**Figure 8**). Compared to 293 cells, significant intracellular red Dox fluorescence and green FMSNPs-CD-PEG-FA fluorescence in HeLa cells were observed after 3 h incubation with the nanoparticles. The observation is in line with our previous results obtained from fluorescence microscopic studies (Figure 6a).

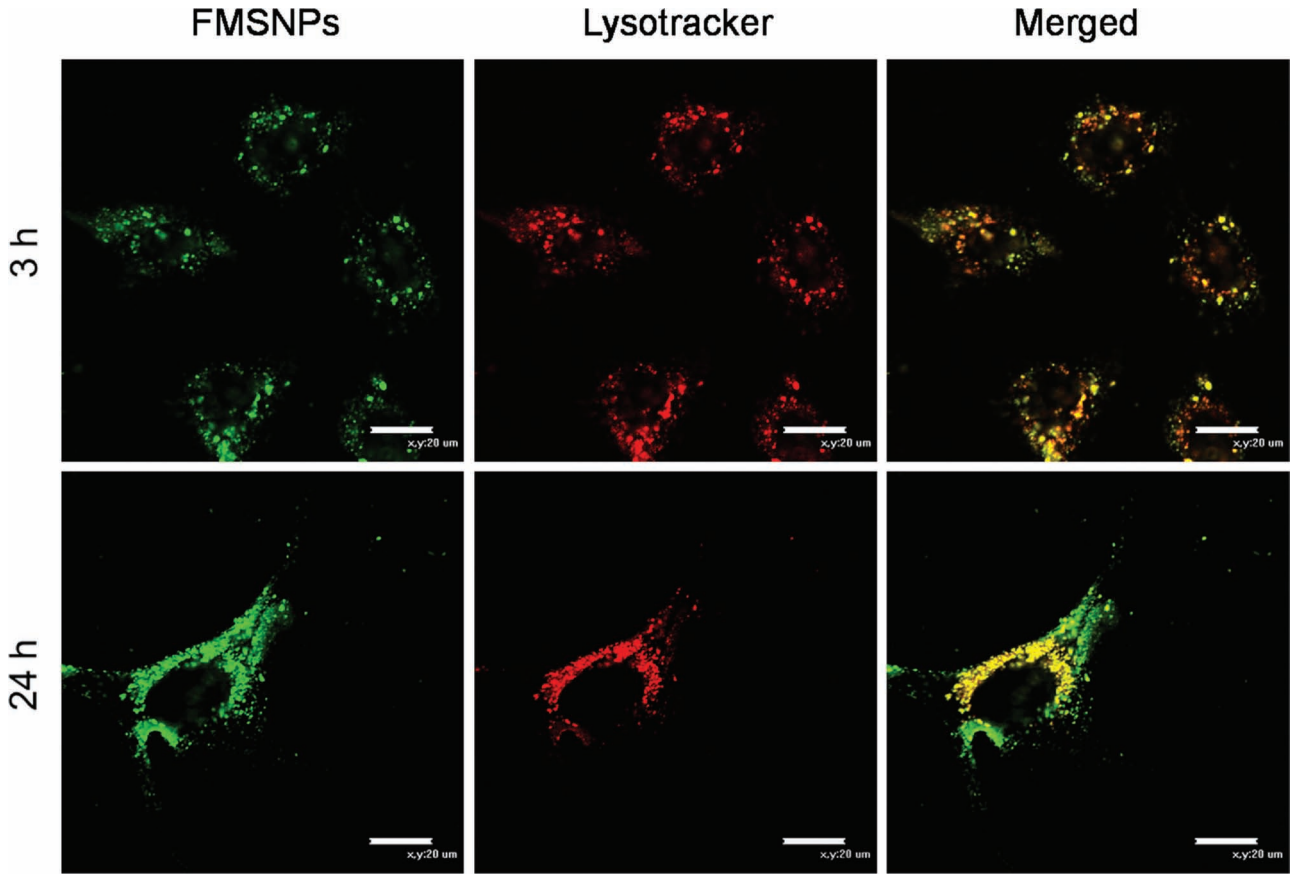

Figure 7. CLSM images of live HeLa cells treated with FMSNPs-CD-PEG-FA for 3 h and 24 h. Lysotracker (red) was used to stain the acidic organelles of the cell. Scale bar: 20 μm.

After 10 h of incubation, more nanoparticles were endocytosed and accumulated at the intracellular location of HeLa cells. This action is followed by the Dox release to the nucleus triggered by acidic endosomal pH and by the reduction of intracellular GSH after 24 h, and the induction of cytotoxicity and the appearance of apoptotic bodies (arrows in Figure 8) after 48 h. In contrast, there is almost no endocytosed nanoparticle observed in 293 normal cells after 10 h, on account of low FR expression on the surface of 293 cells. After 24 h of incubation, a few of nanoparticles were taken up into 293 cells via non-specific endocytosis. Close investigations indicate that there is no observable 293 cell death after 48 h, since only a very small amount of Dox is released into 293 cells (Figure S7 in the SI). The obtained results demonstrate that the introduction of FA ligand can significantly improve specific targeting of MSNPs-S-S-CD into HeLa cancer cells over 293 normal cells, thereby facilitating the Dox release into cancer cells for apoptosis.

2.6. Anticancer Efficacy of Multifunctional MSNPs

Efficient delivery of Dox into cancer cells to increase the intracellular drug concentration can inhibit the cell growth and ultimately lead to the cell death. In addition, non-cytotoxic nanocarriers are desirable in order to avoid side effects in biological systems. Thus, cell viability incubated with MSNPs-CD-PEG-FA was analyzed by the MTS assay in both HeLa and 293 cells. The results reveal that MSNPs-CD-PEG-FA in PBS is not cytotoxic to the cells under the measured concentration range up to 500 μg mL^{-1} (Figure S8 in the SI). However, significant inhibition of cell growth was observed when the cells were treated with Dox-loaded nanoparticles. We individually incubated free Dox, Dox-MSNPs-CD-PEG-FA, and Dox-MSNPs-CD-PEG at different Dox doses with HeLa cells for 24, 48, and 72 h (**Figure 9**a-c). Cytotoxic efficacy of Dox-MSNPs-CD-PEG-FA in HeLa cells is higher than that of Dox-MSNPs-CD-PEG, indicating that the targeting of the nanoparticles into HeLa cells through FR-mediated endocytosis increases the internalization of nanoparticles and thus leads to a high percentage of Dox release. Compared to free Dox, a little bit low cytotoxicity of Dox-MSNPs-CD-PEG-FA in HeLa cells is probably due to the gradual release of Dox within the cells. After 3 h of incubation, stronger red Dox fluorescence was observed in the nucleus of HeLa cells treated with free Dox as compared with that treated with Dox-MSNPs-CD-PEG-FA (Figure S9 in the SI). The Dox release from Dox-MSNPs-CD-PEG-FA was accelerated by the GSH reduction within the cytoplasm of cancer cells after the removal of β-CD capping rings through the cleavage of the pre-installed disulfide bonds.

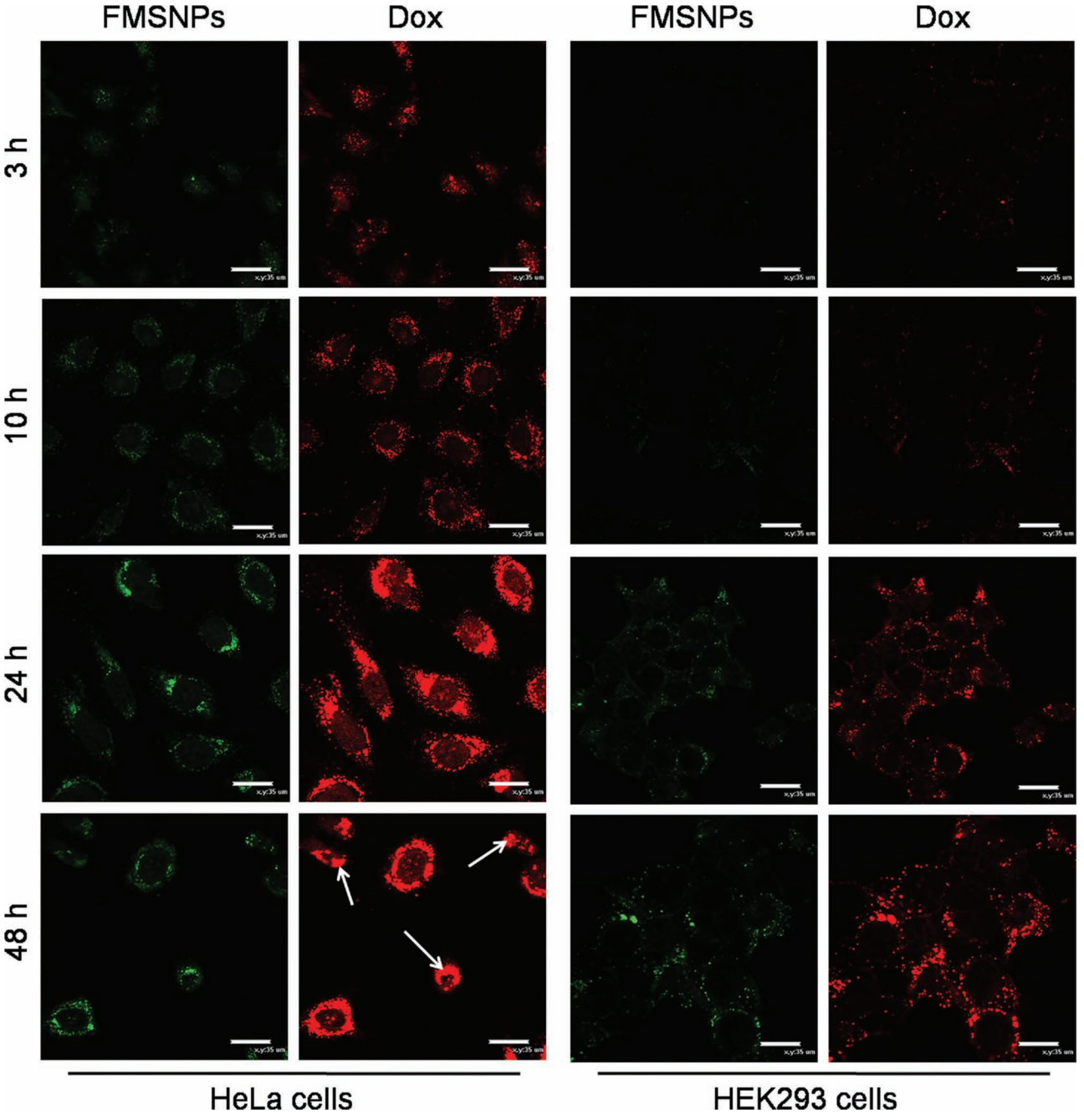

Figure 8. CLSM images of HeLa cells and HEK293 cells incubated with Dox-loaded FMSNPs-CD-PEG-FA under the indicated times. The green fluorescence is from the endocytosed FMSNPs-CD-PEG-FA in the cells, and the red fluorescence is from released Dox and Dox retained within FMSNPs-CD-PEG-FA. Scale bar: 35 μm.

To evaluate further the selectivity of Dox-MSNPs-CD-PEG-FA for cancer cells over normal cells, we also incubated 293 normal cells with free Dox, Dox-MSNPs-CD-PEG-FA, or Dox-MSNPs-CD-PEG at different Dox doses for 24, 48, and 72 h (Figure 9d-f), and then determined the half maximal inhibitory concentration (IC_{50}) of Dox by the MTS assay (**Table 1**). Free Dox shows an obvious cytotoxicity to HeLa cancer cells at a low concentration (IC_{50} = 0.53 ± 0.09 μg mL^{-1}) after incubation for 72 h. However, it also exhibits a high cytotoxicity to 293 normal cells (IC_{50} = 0.55 ± 0.11 μg mL^{-1}) under the same condition. Dox-MSNPs-CD-PEG-FA has a significant cytotoxicity to HeLa cells (IC_{50} = 0.65 ± 0.11 μg mL^{-1}) after incubation for 72 h, whereas a low cytotoxic effect was observed for 293 cells (IC_{50} = 13.56 ± 1.68 μg mL^{-1} for 72 h). Calculated IC_{50} values for the inhibition of cell growth by Dox-MSNPs-CD-PEG-FA and free Dox reveal that cancer cells are 21-fold more sensitive to Dox-MSNPs-CD-PEG-FA as compared with normal cells, while both types of cells are equally sensitive to free Dox. The cancer cell-selective

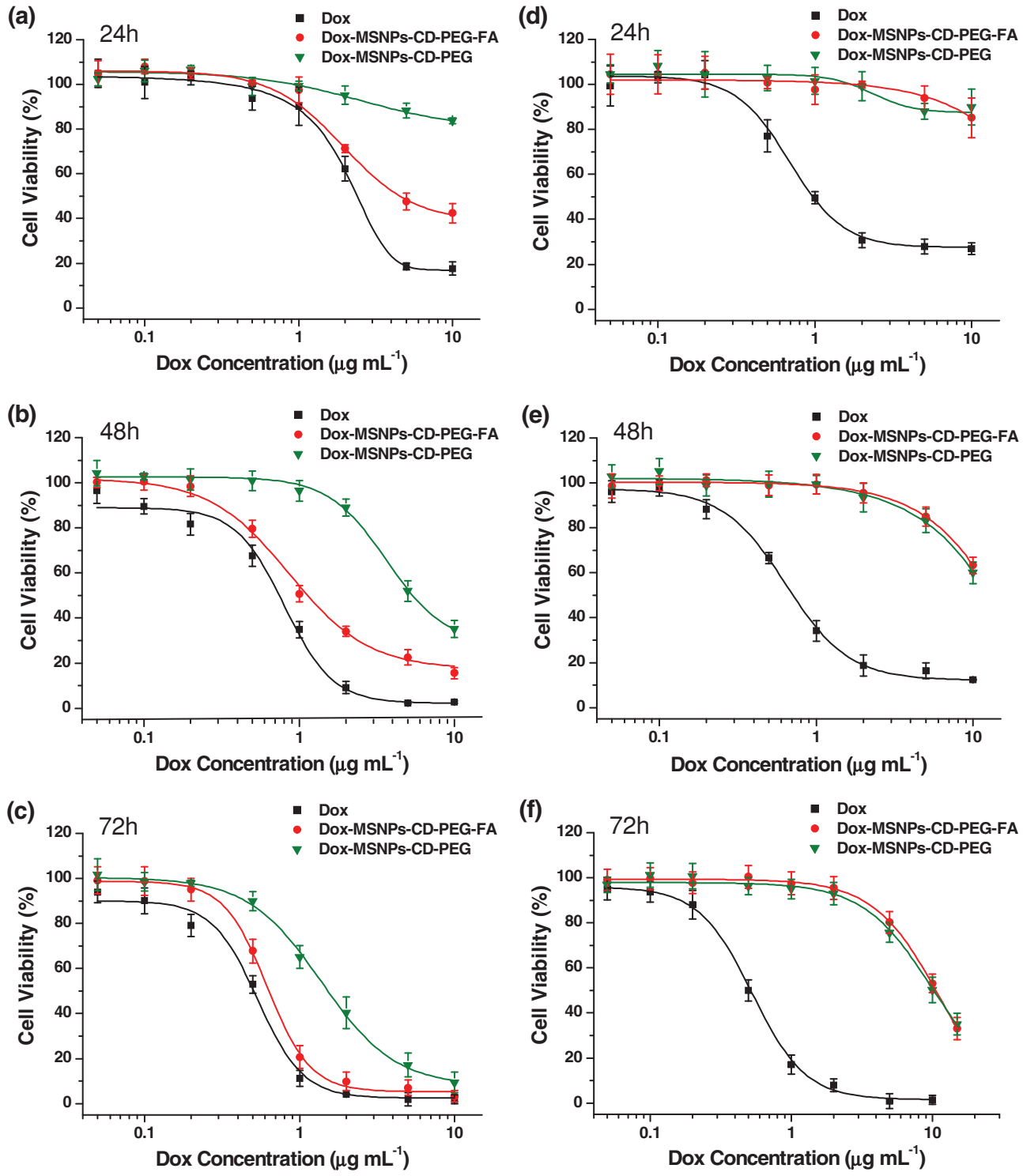

Figure 9. a–e) Viability of HeLa cells (a,b,c) and 293 cells (d,e,f) incubated with free Dox, Dox-MSNPs-CD-PEG-FA, or Dox-MSNPs-CD-PEG at different Dox doses. The cells were exposed to the samples for the indicated times. The data represent the mean values ± the standard deviation (SD) ($n = 3$).

apoptosis of Dox-MSNPs-CD-PEG-FA may be attributed to the cooperative effects of folate-mediated targeting and pH/GSH-triggered Dox release. GSH has a relatively high concentration (1–10 mM) in the cytoplasm and is the major reducing agent in biochemical processes.[48] The intracellular Dox release from Dox-MSNPs-CD-PEG-FA can be triggered by GSH in the cytoplasm of cancer cells, because the intracellular GSH level in cancer cells has been found to be higher than that in normal

Table 1. Half-maximal inhibitory concentrations (IC_{50}, mean ± SD) of free Dox, Dox-MSNPs-CD-PEG-FA, and Dox-MSNPs-CD-PEG after 72 h incubation with cells.

Cell line	Dox [μg mL^{-1}]	Dox-MSNPs-CD-PEG-FA [μg mL^{-1}]	Dox-MSNPs-CD-PEG [μg mL^{-1}]
HeLa cancer cells	0.53 ± 0.09	0.65 ± 0.11	1.26 ± 0.32
293 normal cells	0.55 ± 0.11	13.56 ± 1.68	11.84 ± 1.71

cells.[49,50] We observed a high intracellular Dox release from Dox-MSNPs-CD-PEG-FA within HeLa cells when compared with 293 cells (Figure S7 in the SI). Moreover, we found that the cytotoxicity of Dox-MSNPs-CD-PEG-FA to 293 normal cells can be significantly enhanced (**Figure 10**) after 293 cells were treated with glutathione monoester (GSH-OEt, 5 mM), a compound which can be efficiently internalized into cells and hydrolyzed to generate GSH.[48] In addition, the enhanced apoptotic effects of Dox-MSNPs-CD-PEG-FA to cancer cells were also confirmed in the case of MDA-MB-231 breast cancer cells when compared with MCF-10A breast normal cells (Figure S10 in the SI). All these results reveal that the enhanced drug delivery efficacy of multifunctional nanoparticles is due to the cooperative effects of folate-mediated targeting and stimuli-triggered drug release.

Chemotherapeutic drugs are well-known for their adverse side effects such as fatigue, nausea, and hair loss, which are resulted from the way they work to kill quickly dividing cells in the body rather than cancerous cells specifically. Therefore, the combination of cancer targeting with controlled drug release is a more desirable route in the cancer therapy in order to reduce these negative effects to healthy cells. In our current study, multifunctional MSNPs can be efficiently trapped by HeLa cancer cells through receptor-mediated endocytosis. After being taken up by cancer cells, the system can provide a sustained Dox release triggered by acidic endosomal pH. Subsequently, the intracellular Dox release can be further increased by the GSH reduction after the multifunctional nanoparticles escape from the endosome and enter into the cytoplasm of cancer cells. Thus, the multifunctional MSNPs promote the anticancer efficacy of Dox through folate-mediated targeting to cancer cells and subsequent stimuli-triggered drug release.

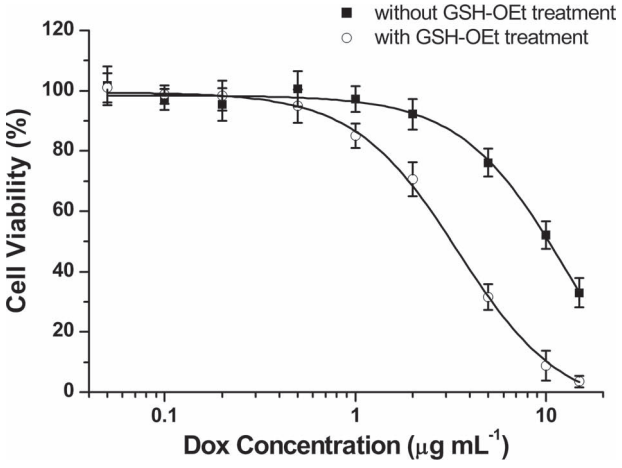

Figure 10. Viability of 293 cells incubated with Dox-MSNPs-CD-PEG-FA at different Dox doses for 72 h. The Dox-induced cytotoxicity was affected by GSH-OEt. The data represent the mean values ± SD (n = 3).

3. Conclusions

In summary, a new generation of multifunctional MSNPs has been developed for both folate-mediated targeting and stimuli-triggered drug delivery. The β-CD$(NH_2)_7$ rings have been attached covalently onto the mesopore orifices and served as caps to block drug molecules within the mesopores. FA-PEG-Ad has been successfully immobilized onto the MSNP system through the Ad/β-CD complexation, offering the folate targeting unit on the surface of the nanoparticles. Such drug-loaded multifunctional MSNPs can significantly inhibit the growth of specific cancer cells, owing to the high efficiency of cellular uptake by receptor-mediated endocytosis and subsequent stimuli-triggered drug release in the cells. We have demonstrated that the apoptosis of cancer cells can be achieved by using single nanoparticle entities featured the combination of folate-mediated targeting and stimuli-triggered drug release. In addition, the introduction of the β-CD$(NH_2)_7$ ring as the mesopore capping agent on MSNPs provides a novel platform for the incorporation of targeting ligands onto the nanocarrier system. This approach presents a general route to introduce certain types of targeting ligands on the MSNP surface for targeted drug delivery.

4. Experimental Section

Materials: Nanopure water (18.2 MΩ; Millipore Co., USA) was used in all experiments and to prepare all buffers. Cetyltrimethylammonium bromide (CTAB), β-cyclodextrin (β-CD), 1-(3-(dimethylamino)propyl)-3-ethylcarbodiimide hydrochloride (EDC·HCl), dithiothreitol (DTT), ethylenediamine, fluorescein isothiocyanate (FITC), glutathione (GSH), and 3-mercaptopropyltrimethoxysilane (MPTMS) were purchased from Alfa Aesar and used as received. 3-Aminopropyltriethoxysilane (APTES) and tetraethylorthosilicate (TEOS) were purchased from Merck and used as received. 1-Adamantanethiol, doxorubicin hydrochloride, and folic acid (FA) were purchased from Sigma-Aldrich and used without further purifications. Maleimide functionalized methoxyl polyethylene glycol (mPEG-MAL, MW = 5 kD), *N*-hydroxysuccinimide (NHS), and maleimide (MAL) hetero-functionalized polyethylene glycol (NHS-PEG-MAL, MW = 5 kD) were purchased from NANOCS Inc (New York, NY). 2-Carboxyethyl-2-pyridyl disulfide was synthesized according to a reported procedure.[51] β-CD$(NH_2)_7$ was synthesized as described previously.[27] RPMI 1640, RPMI 1640 without folic acid, RPMI 1640 without phenol red, fetal bovine serum (FBS), and LysoTracker probes (Red DND-99) were purchased from Invitrogen (Carlsbad, CA, USA). All other chemicals were commercially available and used without further purifications.

Characterizations: ^{1}H NMR spectra were recorded on a Bruker spectrometer operating at 400 MHz. The solid-state spectra were collected on an ECA400 NMR spectrometer (JEOL, 400 MHz), using a 4 mm CP/MAS probe at room temperature. TEM images were collected on a JEOL JEM-1400 instrument operated at 100 kV. TEM samples were prepared by pipetting a drop of nanoparticle aqueous solution onto a 200-mesh copper grid coated with carbon, and the grid was dried under air before the measurement. UV-Vis measurements were performed on a Shimadzu UV3600 spectrometer. Fluorescence spectra were recorded on a Cary Eclipse Fluorescence Spectrophotometer. For the measurement

of Dox emission spectra, emission and excitation band widths were set at 5 nm and 10 nm, respectively. The excitation wavelength was 480 nm, and the emission was recorded in the wavelength range of 500-750 nm. Matrix-assisted laser desorption/ionization time-of-flight (MALDI-TOF) mass spectra were recorded on an ABI 4800 MALDI TOF/TOF mass spectrometer by positive mode electrospray ionization. α-Cyano-4-hydroxycinnamic acid (CHCA) was used as a matrix. N_2 adsorption-desorption isotherms were recorded on a Micromeritics ASAP 2020M automated sorption analyzer. The samples were degassed at 100 °C for 12 h. The specific surface areas were calculated from the adsorption data in low pressure range using the Brunauer-Emmett-Teller (BET) model and pore size was determined following the Barret-Joyner-Halenda (BJH) method. Powder X-ray diffraction (XRD) patterns were collected using a PANalytical X'Pert diffractometer equipped with Cu Kα radiation (λ = 1.5405980 Å). Thermogravimetric analysis was carried out for powder samples using a TGA Q500 recorded from 25 to 790 °C in an air flow at a heating rate of 10 °C min^{-1}. Dynamic light scattering (DLS) and zeta potential experiments were performed at 25 °C using a Malvern ZetaSizer NanoZS instrument, equipped with a He-Ne laser (633 nm) at a fixed scattering angle of 90°. All of the measurements were performed with the nanoparticles suspended in filtered water or filtered cell culture media at a concentration of 50 μg mL^{-1}. The data were analyzed by Malvern Dispersion Technology Software.

Synthesis of mPEG-Ad and FA-PEG-Ad: All syntheses were performed as described in the supporting information.

Synthesis of MSNPs-0 and FITC-labeled MSNPs-0: MSNPs-0 was synthesized as described previously.[37] CTAB (0.25 g, 0.7 mmol) was dissolved in a mixture of distilled H_2O (120 mL) and 2 M NaOH (0.875 mL). The mixture reaction was heated to 80 °C. After the temperature stabilized, TEOS (1.25 mL) was added to the CTAB solution. The solution was stirred vigorously at 80 °C for 2 h. The resulting solid was filtered and washed with excessive double-distilled H_2O and MeOH, respectively. Finally, the sample was dried under vacuum to yield the as-synthesized MSNPs-0.

As for FITC-labeled MSNPs-0, fluorescein isothiocyanate (2.7 mg) was dissolved in absolute EtOH (1.5 mL) and reacted with APTES (6 μL) in the dark for 2 h. CTAB (0.25 g, 0.7 mmol) was dissolved in a mixture of distilled H_2O (120 mL) and 2 M NaOH (0.875 mL), followed by adjusting the solution temperature to 80 °C. TEOS (1.25 mL) and FITC-APTES were then added to the CTAB solution. The mixture was allowed to stir for 2 h to give rise to white precipitates. FITC-labeled MSNPs-0 was obtained by filtration and dried under vacuum.

Synthesis of MSNPs-SH-0: MSNPs-0 (100 mg) was suspended in anhydrous toluene (20 mL) and 3-mercaptopropyltrimethoxysilane (3 mL) was added to the solution. The mixture solution was heated to 120 °C and stirred under N_2 for 12 h. The precipitates were collected by centrifugation (6000 rpm, 10 min), and washed with toluene and methanol.

Synthesis of MSNPs-COOH-0: MSNPs-SH-0 (200 mg) was treated with a solution of 2-carboxyethyl-2-pyridyl disulfide (0.20 g, 0.93 mmol) in EtOH (10 mL) at room temperature under vigorous stirring for 48 h. The resulting MSNPs-COOH-0 was separated by centrifugation (6000 rpm, 10 min), washed with EtOH and dried under vacuum.

Synthesis of MSNPs-S-S-COOH: In order to remove surfactant template (CTAB) from the mesopores of the nanoparticles, MSNPs-COOH-0 was suspended in a mixture of MeOH (50 mL) and concentrated HCl (3 mL, 37.4%), and the solution was heated under reflux for 24 h. The nanoparticles were then filtered and washed extensively with H_2O and MeOH. Finally, the surfactant-removed MSNPs-S-S-COOH was placed under vacuum to remove the remaining solvents in the mesopores.

Drug Loading: MSNPs-S-S-COOH (20 mg) was added to an anhydrous DMF solution (1 mL) containing Dox (4 mg mL^{-1}). After the mixture solution was stirred overnight, it was sonicated to maximize the nanoparticle dispersion. Dox-loaded MSNPs-S-S-COOH was obtained by centrifugation. β-CD$(NH_2)_7$ (30 mg, 0.021 mmol) was then added to an aqueous solution (10 mL) containing Dox-loaded MSNPs-S-S-COOH in the presence of EDC·HCl (15 mg, 0.078 mmol). After the mixture solution was stirred for 48 h, the resulting nanoparticles were collected by centrifugation, washed extensively with PBS buffer solution (pH 7.4), and finally dried under vacuum. The loading percentage of Dox in MSNPs-S-S-CD was estimated through the UV-Vis absorption measurements by subtracting the amount of Dox in the collected supernatant from the total amount of Dox added.

Preparation of Dox-loaded MSNPs-CD-PEG-FA: Dox-loaded MSNPs-S-S-CD (10 mg) was suspended in PBS buffer solution (10 mL, pH 7.4), and then a mixture of mPEG-Ad (10 mg) and FA-PEG-Ad (10 mg) was added to the suspension. The mixture was stirred at room temperature for 24 h. Dox-loaded MSNPs-CD-PEG-FA was obtained by centrifugation, and washed several times with PBS (pH 7.4) and dried under vacuum.

Cell Culture: 293 (human embryonic kidney) cells, HeLa (human cervical cancer) cells, and MDA-MB-231 (breast cancer) cells were cultured in RPMI 1640 medium containing 10% FBS, penicillin (100 U mL^{-1}), streptomycin (100 μg mL^{-1}), and *L*–glutamine (2 mM) in a humidified atmosphere with 5% CO_2 at 37 °C. MCF-10A (breast epithelial) cells were cultured in Dulbecco's Modified Eagle's Medium/F12 (DMEM/F12) (Invitrogen, 11330-032) supplemented with 5% horse serum (Invitrogen, 16050-122), 1% penicillin/streptomycin (Invitrogen, 15070-063), hydrocortisone (0.5 μg mL^{-1}, Sigma, H-0888), cholera toxin (100 ng mL^{-1}, Sigma, C-8052), insulin (10 μg mL^{-1}, Sigma, I-1882), and recombinant human EGF (20 ng mL^{-1}, Peprotech, 100-15).

Flow Cytometric Analysis of Particle Uptake: HeLa cells were seeded into 12-well plate at a density of 1×10^4 cells per well and grown in RPMI 1640 medium (without FA). When the cells reached 90% confluence for 24 h, the medium was removed and the cells were washed twice with PBS buffer solution (pH 7.4). The cells were then treated with FMSNPs-CD-PEG-FA or FMSNPs-CD-PEG in medium at a concentration of 10 μg mL^{-1} and incubated at 37 °C for 3 h. For free FA competition experiments, the cells were cultured with FA (1 mM) for 24 h prior to the addition of nanoparticles. The cells were detached by 0.25% (w/v) trypsin-0.03% (w/v) EDTA solution and the extracellular fluorescence was quenched by re-suspension to trypan blue (200 μg mL^{-1}) at room temperature for 10 min. The cells were washed twice with PBS (1 mL). The amount of endocytosed nanoparticles inside cells was analyzed at FITC-A channel using FACSCalibur flow cytometer (BD Biosciences).

Confocal Laser Scanning Microscopy (CLSM): For cellular internalization observation, HeLa cells were seeded in 35 mm plastic-bottomed μ-dishes and grown in RPMI 1640 medium (without FA) for 24 h. The cells were washed three times with PBS (pH 7.4), and then incubated with FMSNPs-CD-PEG-FA (20 μg mL^{-1}) in the culture medium at 37 °C for 3 or 24 h. The medium was replaced with preheated (37 °C) medium containing LysoTracker (50 nM). After incubation for 30 min, the cells were washed with fresh medium and soaked for 30 min in 0.4% trypan blue (1 mL) in the culture medium. After washing with the medium, the cells were monitored live under a Nikon Eclipse TE2000-E laser-scanning confocal microscope (100 × oil objective, 488/543 nm excitation).

For intracellular Dox release observation, HeLa cells or 293 cells were seeded according to the description abovementioned. The cells were washed three times with PBS, and then incubated with Dox-loaded FMSNPs-CD-PEG-FA (20 μg mL^{-1}) in RPMI 1640 medium at 37 °C for 3, 10, 24, or 48 h. The cells were washed three times with PBS and fixed with fresh 4.0% formaldehyde at room temperature for 15 min. After washing with PBS (pH 7.4), the cells were subjected to the CLSM observation.

Cell Growth Inhibition Assay: The cells were seeded into 96-well plate at a density of 5×10^3 cells per well in a complete RPMI 1640 medium (200 μL), and then incubated in humidified 5% CO_2 atmosphere at 37 °C for 24 h. The culture medium was then replaced with fresh culture medium (200 μL) containing either free Dox or Dox-loaded MSNPs at different Dox doses. The cells were further incubated for 24, 48, or 72 h, and were then washed three times with PBS in order to remove free Dox or nanoparticles. A portion (20 μL) of 3-(4,5-dimethylthiazol-2-yl)-5-(3-carboxymethoxyphenyl)-2-(4-sulfophenyl)-2H-tetrazolium (MTS)/phenazine methosulfate (PMS) solution (20:1, v/v, CellTiter 96® AQueous kit) was added to each well of a 96-well plate containing cells in RPMI 1640 (100 μL) without phenol red. After incubation in humidified 5% CO_2 atmosphere at 37°C for 1 h, the absorbance at 490 nm

was recorded using a microplate reader (infinite M200, TECAN). The spectrophotometer was calibrated to zero absorbance using culture medium without cells. The relative cell viability compared to control wells containing medium without nanoparticles was calculated by $[A]_{test}/[A]_{control}$, where $[A]_{test}$ and $[A]_{control}$ are the average absorbance of the test and control samples, respectively. The IC_{50} values were calculated using GraphPad Prism software (version 5.01), which were based on three independent experiments.

Supporting Information

Supporting Information is available from the Wiley Online Library or from the author.

Acknowledgements

We thank the Singapore National Research Foundation Fellowship (NRF2009NRF-RF001-015) and Nanyang Technological University for financial support.

Received: May 15, 2012
Revised: July 7, 2012
Published online: July 30, 2012

[1] D. Peer, J. M. Karp, S. Hong, O. C. Farokhzad, R. Margalit, R. Langer, *Nat. Nanotechnol.* **2007**, *2*, 751.
[2] F. Danhier, O. Feron, V. Préat, *J. Controlled Release* **2010**, *148*, 135.
[3] J. Panyam, V. Labhasetwar, *Adv. Drug Delivery Rev.* **2003**, *55*, 329.
[4] M. E. Davis, Z. Chen, D. M. Shin, *Nat. Rev. Drug Discovery* **2008**, *7*, 771.
[5] K. Riehemann, S. W. Schneider, T. A. Luger, B. Godin, M. Ferrari, H. Fuchs, *Angew. Chem.* **2009**, *121*, 886; *Angew. Chem. Int. Ed.* **2009**, *48*, 872.
[6] C. Kim, S. S. Agasti, Z. Zhu, L. Lsaacs, V. M. Rottello, *Nat. Chem.* **2010**, *2*, 962.
[7] Y. M. Yang, J. X. Aw, K. Chen, F. Liu, P. Padmanabhan, Y. L. Hou, Z. Cheng, B. G. Xing, *Chem. Asian J.* **2011**, *6*, 1381.
[8] V. P. Torchilin, *Nat. Rev. Drug Discovery* **2005**, *4*, 145.
[9] F. E. Alemdaroglu, N. C. Alemdaroglu, P. Langguth, A. Herrmann, *Adv. Mater.* **2008**, *20*, 899.
[10] N. Doshi, S. Mitragotri, *Adv. Funct. Mater.* **2009**, *19*, 3843.
[11] M. Motomov, Y. Roiter, I. Tokarev, S. Minko, *Prog. Polym. Sci.* **2010**, *35*, 174.
[12] D. Farrell, J. Alper, K. Ptak, N. J. Panaro, P. Grodzinski, A. D. Barker, *ACS Nano* **2010**, *4*, 589.
[13] Q. He, Z. Zhang, F. Gao, Y. Li, J. Shi, *Small* **2011**, *7*, 271.
[14] H. Meng, M. Xue, T. Xia, Z. Ji, D. Y. Tarn, J. I. Zink, A. E. Nel, *ACS Nano* **2011**, *5*, 4131.
[15] E. Wagner, *Expert Opin. Biol. Ther.* **2007**, *7*, 587.
[16] P. M. Friden, L. R. Walus, G. F. Musso, M. A. Taylor, B. Malfroy, R. M. Starzyk, *Proc. Natl. Acad. Sci. USA* **1991**, *88*, 4771.
[17] E. Ruoslahti, *Annu. Rev. Cell. Dev. Biol.* **1996**, *12*, 697.
[18] M. Prabaharan, J. J. Grailer, S. Pila, D. A. Steeber, S. Gong, *Biomaterials* **2009**, *30*, 3009.
[19] S. Saha, K. C. F. Leung, T. D. Nguyen, J. F. Stoddart, J. I. Zink, *Adv. Funct. Mater.* **2007**, *17*, 685.
[20] J. M. Rosenholm, C. Sahlgren, M. Lindén, *Nanoscale* **2010**, *2*, 1870.
[21] M. W. Ambrogio, C. R. Thomas, Y. L. Zhao, J. I. Zink, J. F. Stoddart, *Acc. Chem. Res.* **2011**, *44*, 903.
[22] F. Torney, B. G. Trewyn, V. S. Y. Lin, K. Wang, *Nat. Nanotechnol.* **2007**, *2*, 295.
[23] T. D. Nguyen, H. R. Tseng, P. C. Celestre, A. H. Flood, Y. Liu, J. F. Stoddart, J. I. Zink, *Proc. Natl. Acad. Sci. USA* **2005**, *102*, 10029.
[24] R. Liu, X. Zhao, T. Wu, P. Feng, *J. Am. Chem. Soc.* **2008**, *130*, 14418.
[25] T. D. Nguyen, Y. Liu, S. Saha, K. C. F. Leung, J. F. Stoddart, J. I. Zink, *J. Am. Chem. Soc.* **2007**, *129*, 626.
[26] H. Kim, S. Kim, C. Park, H. Lee, H. J. Park, C. Kim, *Adv. Mater.* **2010**, *22*, 4280.
[27] Y. L. Zhao, Z. Li, S. Kabehie, Y. Y. Botros, J. F. Stoddart, J. I. Zink, *J. Am. Chem. Soc.* **2010**, *132*, 13016.
[28] H. Meng, M. Xue, T. Xia, Y. L. Zhao, F. Tamanoi, J. F. Stoddart, J. I. Zink, A. E. Nel, *J. Am. Chem. Soc.* **2010**, *132*, 12690.
[29] H. P. Rim, K. H. Min, H. J. Lee, S. Y. Jeong, S. C. Lee, *Angew. Chem.* **2011**, *123*, 9015; *Angew. Chem. Int. Ed.* **2011**, *50*, 8853.
[30] A. Schlossbauer, J. Kecht, T. Bein, *Angew. Chem.* **2009**, *121*, 3138; *Angew. Chem. Int. Ed.* **2009**, *48*, 3092.
[31] A. Bernardos, E. Aznar, M. D. Marcos, R. Martínez-Máñez, F. Sancenón, J. Soto, J. M. Barat, P. Amorós, *Angew. Chem.* **2009**, *121*, 5998; *Angew. Chem. Int. Ed.* **2009**, *48*, 5884.
[32] C. Park, H. Kim, S. Kim, C. Kim, *J. Am. Chem. Soc.* **2009**, *131*, 16614.
[33] C. Park, K. Lee, C. Kim, *Angew. Chem.* **2009**, *121*, 1301; *Angew. Chem. Int. Ed.* **2009**, *48*, 1275.
[34] Y. Bae, S. Fukushima, A. Harada, K. Kataoka, *Angew. Chem.* **2003**, *115*, 4788; *Angew. Chem. Int. Ed.* **2003**, *42*, 4640.
[35] S. Ganta, H. Devalapally, A. Shahiwala, M. Amiji, *J. Controlled Release* **2008**, *126*, 187.
[36] E. S. Lee, Z. Gao, Y. H. Bae, *J. Controlled Release* **2008**, *132*, 164.
[37] Q. Cai, Z. S. Luo, W. Q. Pang, Y. W. Fan, X. H. Chen, F. Z. Cui, *Chem. Mater.* **2001**, *13*, 258.
[38] B. Zhang, R. Breslow, *J. Am. Chem. Soc.* **1993**, *115*, 9353.
[39] M. E. Davis, *Mol. Pharmaceutics* **2009**, *6*, 659.
[40] Y. Lu, P. S. Low, *Adv. Drug Delivery Rev.* **2002**, *54*, 675.
[41] J. Sudimack, R. J. Lee, *Adv. Drug Delivery Rev.* **2000**, *41*, 147.
[42] C. Peng, H. Zhang, J. Yu, Q. Meng, L. Fu, H. Li, L. Sun, X. Guo, *J. Phys. Chem. B* **2005**, *109*, 15278.
[43] R. Casasús, M. D. Marcos, R. Martínez-Máñez, J. V. Ros-Lis, J. Soto, L. A. Villaescusa, P. Amorós, D. Beltrán, C. Guillem, J. Latorre, *J. Am. Chem. Soc.* **2004**, *126*, 8612.
[44] J. Lu, M. Liong, J. I. Zink, F. Tamanoi, *Small* **2007**, *3*, 1341.
[45] I. Slowing, B. G. Trewyn, V. S. Y. Lin, *J. Am. Chem. Soc.* **2006**, *128*, 14792.
[46] O. Boussif, F. Lezoualc'h, M. A. Zanta, M. D. Mergny, D. Scherman, B. Demeneix, J. P. Behr, *Proc. Natl. Acad. Sci. USA* **1995**, *92*, 7297.
[47] Y. B. Lim, S. M. Kim, Y. Lee, W. K. Lee, T.-G. Yang, M.-J. Lee, H. Suh, J.-S. Park, *J. Am. Chem. Soc.* **2001**, *123*, 2460.
[48] R. Hong, G. Han, J. M. Fernández, B. Kim, N. S. Forbes, V. M. Rotello, *J. Am. Chem. Soc.* **2006**, *128*, 1078.
[49] G. Saito, J. A. Swanson, K. D. Lee, *Adv. Drug Delivery Rev.* **2003**, *55*, 199.
[50] A. Gupte, R. J. Mumper, *Cancer Treat. Rev.* **2009**, *35*, 32.
[51] J. Carlsson, H. Drevin, R. Axén, *Biochem. J.* **1978**, *173*, 723.